

Petschek reconnection with a nonlocalized resistivity

H. Baty,^{1,a)} T. G. Forbes,^{2,b)} and E. R. Priest^{3,c)}

¹*Observatoire Astronomique de Strasbourg, 11, rue de l'Université, 67000 Strasbourg, France*

²*Institute for the Study of Earth, Oceans, and Space, University of New Hampshire, New Hampshire 03824, USA*

³*Institute of Mathematics, University of St. Andrews, Fife KY169SS, Scotland, United Kingdom*

(Received 14 October 2008; accepted 9 December 2008; published online 15 January 2009)

The impact of using a nonlocalized electrical resistivity having a spatially asymmetric profile is considered on two-dimensional steady-state magnetic reconnection. Starting from an initial Harris current sheet, time-dependent magnetohydrodynamic simulations are carried out over an entire spatial domain without any symmetry assumptions. It is shown that a stationary Petschek-like reconnection is obtained in the half-plane where a uniform resistivity is adopted. The latter configuration is maintained by a coexisting Petschek configuration that is formed in the second half-plane where the resistivity exhibits a classical exponentially decreasing variation. The structure of the central diffusion region is asymmetric, with a stagnation point flow which does not coincide with the X -point. These results suggest conditions under which a Petschek solution can indeed exist in the presence of a small uniform resistivity in the whole domain. © 2009 American Institute of Physics. [DOI: 10.1063/1.3062833]

I. INTRODUCTION

Magnetic field reconnection is a fundamental process in space and astrophysical plasmas, which allows a change in field topology with the conversion of magnetic energy into heating and acceleration of plasma. Two-dimensional magnetohydrodynamic (MHD) reconnection can now be said to be fairly well understood, and the more recent studies are mainly focusing on three-dimensional aspects.¹

However, there is one controversial aspect that, even now, remains puzzling. It concerns the existence of the fast reconnection regime allowed by the Petschek's mechanism.² Numerical MHD simulations have failed to obtain a Petschek-like solution when they use a spatially uniform resistivity. In contrast, Petschek reconnection can be produced when a nonuniform resistivity enhanced at the X -point of the central diffusion region is adopted. In the original model of Petschek, no assumption was made about the spatial dependence of the resistivity, and this led to the suggestion that the Petschek model may be incorrect for a uniform resistivity (see Kulsrud³ and references therein, and Biskamp⁴). This point is not purely academic, since the answer could be of great importance for understanding general aspects of magnetic reconnection in two and three dimensions as well. Furthermore, fast reconnection rates are needed to explain the rapid release of magnetic energy which occurs in phenomena such as solar flares. Note that in this paper, we focus on the MHD approach, which applies to collisional plasmas such as the low solar atmosphere.

In a previous paper (referenced as Paper 1 below),⁵ using MHD experiments, we have found that Petschek reconnection is likely to occur when a quasi-uniform resistivity is employed. Petschek's mechanism possesses four standing

slow-mode shocks attached to the corners of the central diffusion region (see Fig. 1). This is in contrast to the Sweet-Parker model,^{6,7} where the reconnection is much slower, and the diffusion layer is long and occupies the whole of the boundary between opposing magnetic fields. In a Petschek configuration, most of the magnetic energy conversion occurs through the shocks structure. However, the solution obtained in Paper 1 is strongly influenced by the resistivity gradient in the vicinity of the X -point, which is rather small for profiles having a weak nonuniformity. As a consequence, the reconnection rate is far from the maximum rate given by Petschek's famous formula

$$M_e = \pi / (8 \ln R_{me}), \quad (1)$$

where R_{me} and M_e are the magnetic Reynolds number and Alfvén Mach number (i.e., ratio of plasma velocity to the Alfvén speed) of the plasma flowing into the current sheet, respectively. In this sense, the solution obtained in this way can not be considered as so fast.

In the present paper, we continue our previous work by carrying out new MHD experiments. More precisely, following the same numerical procedure, we extend our previous work (where only one quadrant with symmetry assumptions was adopted) to computations over an entire spatial domain. This allows us to set up the solution without any symmetry assumptions. Second, we can adopt an asymmetric resistivity profile with respect to the $y=0$ axis. As a particular case, we are able to investigate reconnection solutions with uniform resistivity in one half part of the full domain independently of the resistivity profile chosen for the second-half part of the domain. This provides new insights on the conditions necessary to set up and maintain a Petschek solution with uniform resistivity, and having a rate closer to the maximum one [given by Eq. (1)] than obtained in Paper 1.

^{a)}Electronic mail: baty@astro.u-strasbg.fr.

^{b)}Electronic mail: terry.forbes@unh.edu.

^{c)}Electronic mail: eric@mcs.st-and.ac.uk.

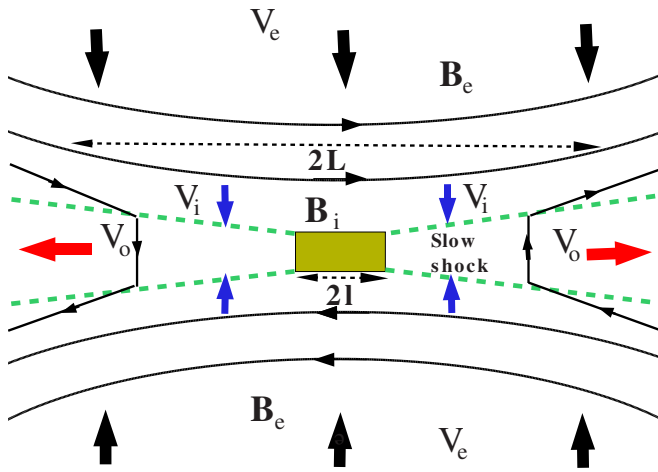


FIG. 1. (Color online) Petschek configuration. A small central current diffusion region is extended outwards by two pairs of standing slow-mode shocks. The inflow plasma velocity is mainly along the x direction, and is denoted by V_e and V_i far from and close to the central region, respectively. The outflow velocity (directed mainly along the y direction) is V_o . When approaching the diffusion region from the inflow boundary (situated at $x = \pm L_x$), the magnetic field amplitude varies from B_e to B_i . The half-length of the diffusion region l is much smaller than the dimension of the whole domain $L=L_y$.

This paper is organized as follows. In Sec. II, we present the model and numerical setup used in this work. The results are shown in Sec. III. Finally, we end with a conclusion in Sec. IV.

II. MODEL AND NUMERICAL SETUP

The setup of the experiments follows previous papers, in which one assumes initially a classical Harris current sheet configuration, with a magnetic field parallel to the y axis and varying with x ,

$$\mathbf{B} = B_e \tanh(x/a)\mathbf{y}, \quad (2)$$

where B_e is the amplitude of the field and a is the initial half-width of the current sheet. A static equilibrium with an isothermal medium is considered. We set the ratio of specific heats γ equal to $5/3$, and choose units such the magnetic permeability is one. We set $B_e=1$, and $a=0.1$, to define our normalization. A rather moderate value at the boundary $x = \pm L_x$ of the plasma β is also chosen; namely, $\beta=0.35$. The initial plasma pressure and density are then set to be $p(x)=1.25-B_e^2/2$ and $\rho(x)=2p(x)/\beta$, respectively.

We solve the usual full set of nonlinear MHD resistive equations as an initial value problem, in two spatial dimensions and Cartesian geometry (x,y) . A total of 200×200 spatial grid points is used in the spatial domain $-L_x \leq x \leq L_x$ and $-L_y \leq y \leq L_y$, of dimensions $L_x=1$ and $L_y=2$. A nonuniform spacing with a grid accumulation is chosen in order to have sufficient cells to resolve the central current sheet. Typically, we are able to achieve a minimum grid spacing of $\Delta x=1.5 \times 10^{-3}$ and $\Delta y=3 \times 10^{-3}$ in the x and y directions, respectively.

The boundary conditions are imposed through the use of two ghost cells situated slightly outside the computational domain at each boundary. Following Paper 1, a procedure

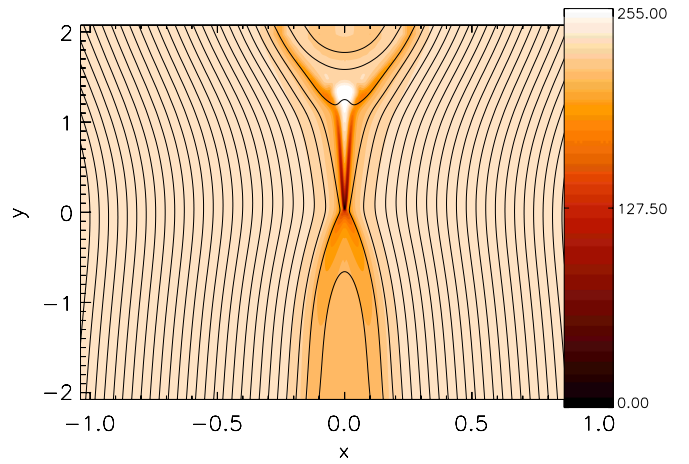


FIG. 2. (Color online) Magnetic field lines and current density structures during the buildup of the solution before the final steady-state configuration has been reached, using an asymmetric resistivity with $\eta_0=10^{-3}$.

with overspecified boundary conditions at the inflow boundary $x = \pm L_x$ is used. More precisely, five conditions are imposed on five physical quantities to be fixed in time and equal to their initial values; namely, the mass density, two components of the flow velocity, the y component of the magnetic field, and the total energy density. In this way, it has been shown that the system is able to choose its own solution without been driven by an external forcing, as required by Petschek-type reconnection.⁸ Additionally, free conditions are also imposed at the outflow boundaries $y = \pm L_y$.

We use the general finite-volume based Versatile Advection Code (VAC,⁹ and select the explicit one-step total variation diminishing scheme with minmod limiting.^{10,11} This is a second-order accurate shock-capturing method making use of a Roe-type approximate Riemann solver. To handle the solenoidal constraint on the magnetic field $\nabla \cdot \mathbf{B}=0$, our VAC simulations apply a projection scheme at every time step in order to remove any numerically generated divergence of the magnetic field up to a predefined accuracy.¹²

In this work, in the half-plane $y \geq 0$, the applied numerical resistivity profile has the following form,

$$\eta(x,y) = (\eta_0 - \eta_1) \exp[-(x/l_x)^2 - (y/l_y)^2] + \eta_1, \quad (3)$$

where η_0 and η_1 are the resistivities at the center of the domain and of the background region, respectively. l_x and l_y are the characteristic length scales of the resistivity variation. In this work, l_y can vary from case to case. This is in contrast to the l_x value, which is taken to be fixed to $l_x=0.05$, as it has been previously shown that its value does not influence the solution (see Paper 1).

III. RESULTS

The use of the resistivity profile given by Eq. (3) for $y \geq 0$, together with a uniform resistivity $\eta = \eta_0$ for the second half-plane $y \leq 0$, is sufficient to produce a Petschek-like configuration in the whole domain. This is illustrated in Figs. 2 and 3, using $\eta_0=10^{-3}$ and $\eta_1=3 \times 10^{-5}$ (the value η_1 is chosen in order to slightly dominate the estimated residual

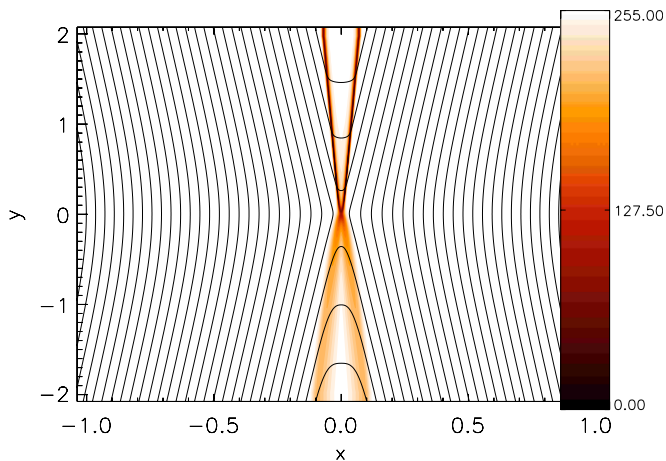


FIG. 3. (Color online) Magnetic field lines and current density for the final steady-state configuration, using an asymmetric resistivity with $\eta_0=10^{-3}$.

numerical resistivity for the spatial resolution used). A value $l_y=0.02$ is also taken for the present asymmetric run.

Figure 2 clearly shows that shocks are first produced in the upper half-plane (where the resistivity is nonuniform). Later, once a Petschek solution is set up in the upper part, another Petschek solution is driven in the bottom half-plane (where the resistivity is constant), as one can see in Fig. 2. In this way, a steady-state reconnection solution has been set up, that appears to be very similar to the schematic view of Fig. 1. However, one must note that shocks are thicker in the lower half-plane due to the higher resistivity employed there (more than one order of magnitude higher than the background resistivity taken for $y \geq 0$).

We have examined in more detail the structure of this final steady-state solution. Using a $y=0$ cut, in Figs. 4 and 5 (for V_x and B_y as a function of the x coordinate), we are able to investigate the transverse structure. Indeed, the transverse variations obtained for the asymmetric run are very similar to the ones corresponding to steady-state Petschek reconnection

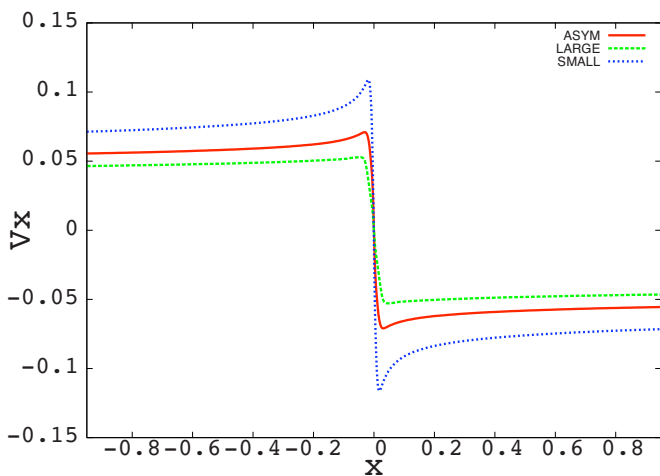


FIG. 4. (Color online) The steady-state x component of the inflow velocity $V_x(x)$ (using a $y=0$ cut) for runs using three different resistivity profiles: an asymmetric resistivity (ASYM, plain line), a symmetric exponential one with $l_y=0.02$ (SMALL, dotted line), and a symmetric exponential case using $l_y=0.2$ (LARGE, dashed line).

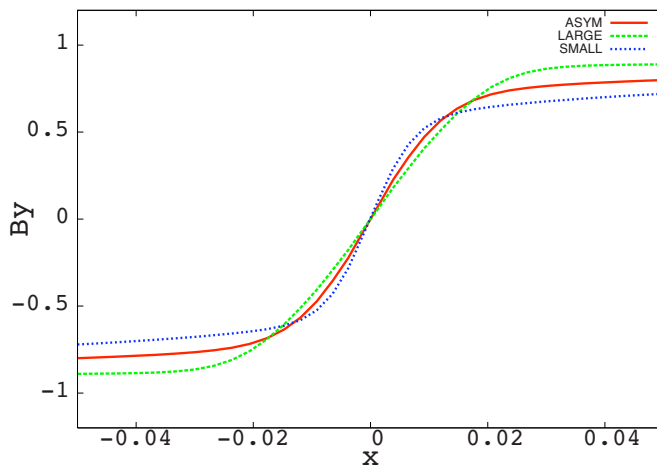


FIG. 5. (Color online) Same as Fig. 4 for the $B_y(x)$ component.

obtained in two simulations using a classical symmetric exponentially decreasing resistivity profile (with $l_y=0.02$ and $l_y=0.2$) for the whole x - y plane. Petschek reconnection, as described in Yan *et al.* for example,¹³ exhibits a decreasing magnetic field amplitude when approaching the diffusion region from the inflow boundary. At the same time, the plasma flow is converging and shows the characteristic variation displayed in Fig. 4.

Moreover, we can deduce from Figs. 4 and 5 that the asymmetric case is intermediate between the two symmetric ones. More precisely, we have checked that our asymmetric solution is very close to a symmetric one using $l_y=0.1$. In contrast to solutions obtained for quasi-uniform resistivity in Paper 1, the Petschek-like solution that is produced in this way has a reconnection rate that is close to the maximum rate given by Petschek’s formula [Eq. (1)]. We nevertheless argue that the rate should depend on the resistivity gradient assumed in the nonuniform resistivity half-plane.

It is also instructive to investigate the longitudinal structure of the steady-state configuration by using $x=0$ cuts. In

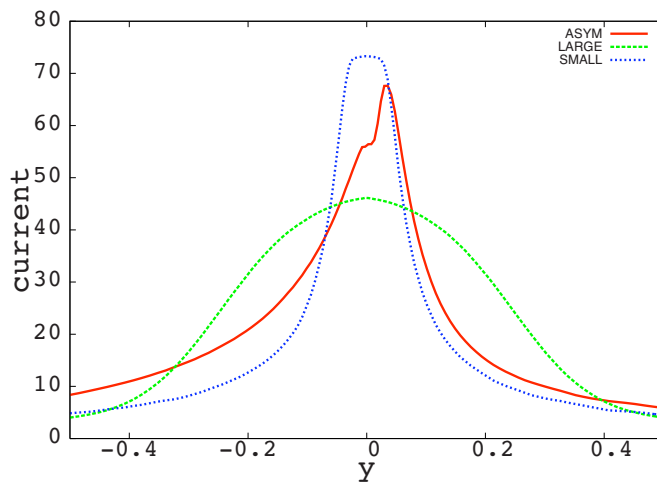
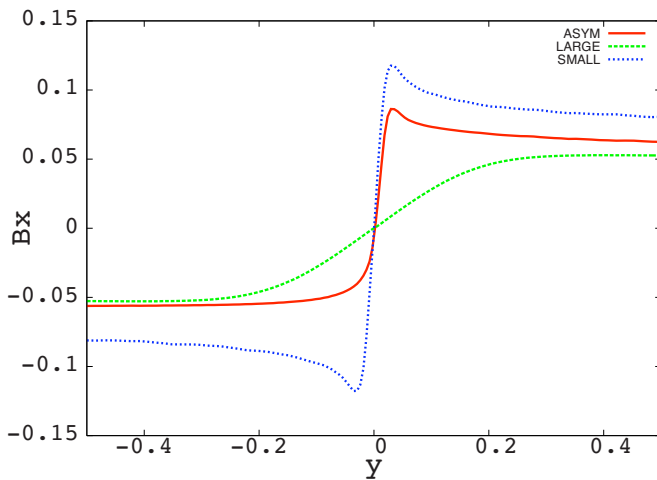
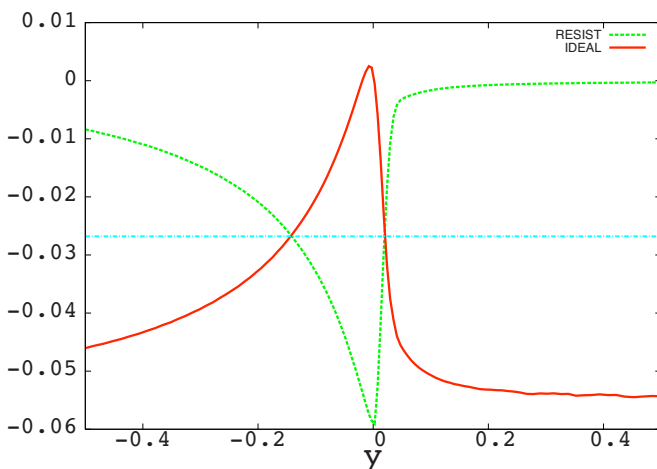
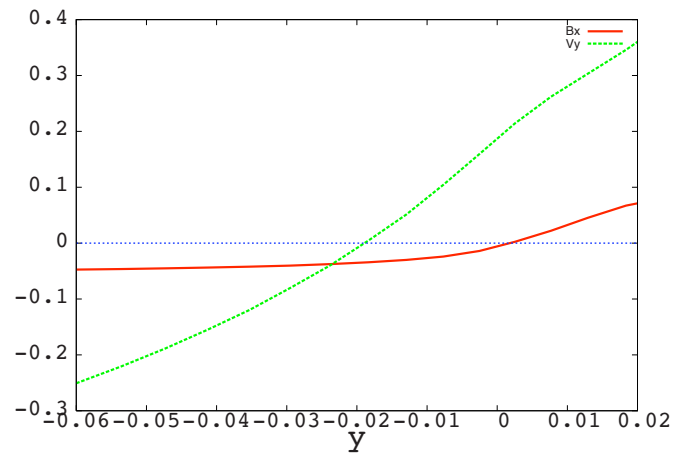


FIG. 6. (Color online) The steady-state current density (using an $x=0$ cut) for three runs using three different resistivity profiles: an asymmetric resistivity (ASYM, plain line), a symmetric exponential case using $l_y=0.02$ (SMALL, dotted line), and a symmetric exponential case using $l_y=0.2$ (LARGE, dashed line).

FIG. 7. (Color online) Same as Fig. 6 for the $B_x(y)$ component.

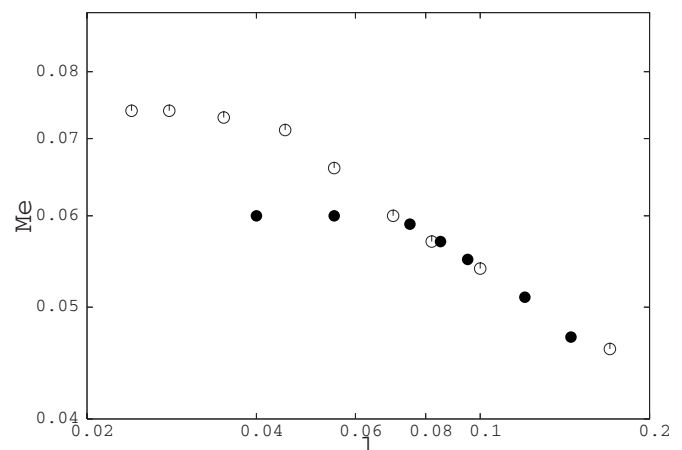
particular, the asymmetric nature of the solution is clearly visible in Figs. 6 and 7. The current density profile displays a maximum amplitude that is shifted from the central location $x=y=0$, to a location in the upper ($y \geq 0$) plane. Again, the solution appears to be intermediate between the two symmetric solutions. Moreover, as the configuration obtained for the asymmetric case is globally different from the solution obtained for the symmetric case with $l_y=0.02$ (using the same resistivity profile in the upper half-plane), this clearly indicates that the solution for $y \geq 0$ is also influenced by the uniform resistivity taken in the lower half-plane. However, in spite of this local asymmetry, one must note that the configuration is nearly symmetric at large scale. Indeed, for example, the outflow velocity of the plasma V_o is the same at the two outflow boundaries; namely, at $y=L_y$ and $y=-L_y$.

In order to explore in somewhat more depth the structure of the diffusion region, we have plotted in Fig. 8, the y variation (for an $x=0$ cut) of the two terms, $V_y B_x$ and ηJ , which are the main purely ideal and resistive contributions to the electrical field $\mathbf{E} = \eta \mathbf{J} + \mathbf{v} \times \mathbf{B}$. For a steady-state configura-

FIG. 8. (Color online) The steady-state $V_y B_x$ (IDEAL, plain line) and ηJ (RESIST, dashed line) terms as a function of the longitudinal coordinate (using a $x=0$ cut). A horizontal line indicates the spatial locations where the two terms are equal.FIG. 9. (Color online) Same as Fig. 8 for the V_y (dashed line) and B_x (plain line) components.

tion the electrical field is uniform by virtue of Faraday's law. The latter plot clearly shows a strong asymmetry, that is particularly visible in the spatial y -locations where the two terms balance. These are for $y=0.02$ in the upper half-plane, and for $y=-0.15$ in the bottom half-plane. As it also corresponds to the two boundaries of the central diffusion region (where the resistive term dominates the ideal convective effect), it indicates that the diffusion region is strongly asymmetric. Figure 9, showing the y profiles of V_y and B_x in this central region, gives us an additional striking feature. The stagnation point flow (where $V_y=0$) is situated at $y=-0.02$, and consequently does not coincide with the magnetic X-point (where $B_x=0$) situated at $y=0$. This is associated with the fact that the y component of the thermal pressure gradient does not vanish at the X-point.

It is instructive to study the dependence of the reconnection rate M_e as a function of the half-length l of the central diffusion region for a given resistivity η_0 . Several (symmetric and asymmetric) cases are thus simulated by varying the l_y parameter for $\eta_0=10^{-3}$. The results are plotted in Fig. 10. The l value is measured by taking the y half-length of the region situated between the two boundaries where the ideal

FIG. 10. Dependence of the reconnection rate M_e on the diffusion region half-length l for $\eta_0=10^{-3}$, using symmetric (nonfilled circles) and asymmetric resistivity profiles (filled circles).

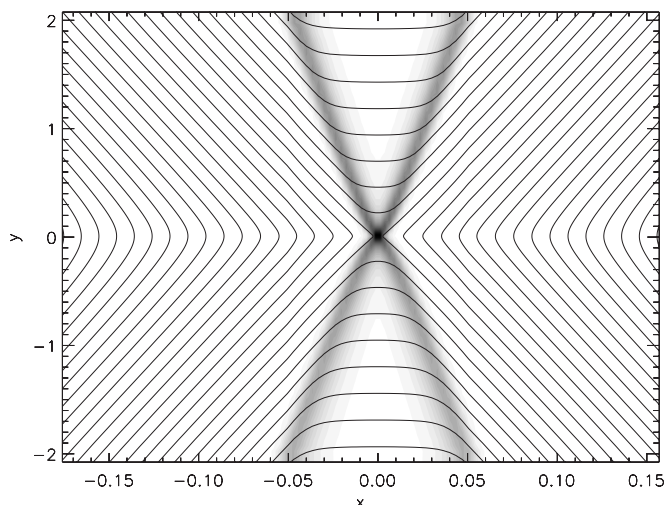


FIG. 11. Magnetic field lines and current density (gray-scale) structures for a final steady-state configuration, using an asymmetric resistivity with $\eta_0=10^{-4}$. Only a part of the whole domain is shown.

and resistive terms ($V_y B_x$ and ηJ) balance (see also Fig. 8). The dependence for the symmetric runs is similar to the results obtained in a previous study by Scholer,¹⁴ showing the existence of a maximum rate (with $M_e \approx 0.074$) when an optimal l value $l \approx 0.04$ is reached. This behavior is also consistent with the original work done by Petschek for obtaining of the maximum rate [given by Eq. (1)].² Figure 10 shows that the asymmetric cases follow a similar global dependence. However, the asymmetry slightly modifies the maximum rate (a value of 0.06 is obtained) that is reached now for $l \approx 0.07$. Note also that the maximum measured values for M_e are substantially higher than predicted by Eq. (1) (a theoretical value of 0.052 is expected for $R_e=2000$), which is valid in the limit of very large Reynold numbers.

Finally, as a relatively high value for the resistivity was used above, we have repeated an additional asymmetric reconnection, but using instead a lower ambient resistivity $\eta_0=10^{-4}$. The results are very similar to the case $\eta_0=10^{-3}$, except that the asymmetry is now weaker and the shocks are thinner, as shown by Fig. 11.

IV. CONCLUSION

We have shown that it is possible to obtain Petschek-like reconnection in a half-plane where a uniform resistivity is imposed. This is helped by a Petschek solution produced in the other half-plane where a classical decreasing resistivity profile is adopted. In this way, a uniform-resistivity solution appears to be driven and maintained by a coexisting nonuniform-resistivity Petschek configuration. Conversely, the nonuniform part of the solution is also influenced by its uniform counterpart. We can therefore imagine that, in principle, a Petschek solution could possibly exist for a uniform-resistivity in the whole domain, but it is probably marginally

stable since an external/internal agent is necessary to maintain it. We plan to investigate this possibility further in the future.

The examination of the whole configuration indicates an asymmetric structure, which is particularly noticeable for the diffusion region. An interesting feature is that the stagnation point and X-point are not co-located. Thus, we can imagine the production of a uniform resistivity solution (for the whole domain) by decoupling these two points. A potential way to realize it would be to employ a specific well-tailored viscosity profile. Indeed, as in previous works, no explicit viscosity was used in the present work. Thus, the viscosity in the present runs is mainly due to the numerical diffusion and is consequently negligible. In a real plasma (like the solar corona, for example), there is no reason to neglect the viscosity compared to the resistivity value. Another possibility for decoupling the stagnation point flow from the X-point could be by the use of obstacles in the flow along the diffusion region.

Finally, we have employed a rather unrealistic resistivity profile in the present study. However, our aim was not to reproduce a magnetic reconnection occurring in a given particular physical context, but instead to demonstrate under which conditions the Petschek process is in principle possible when the resistivity is spatially uniform.

ACKNOWLEDGMENTS

The numerical simulations in this paper have been performed using the Versatile Advection Code maintained by G. Tóth and R. Keppens (see <http://www.phys.uu.nl/toth/>). The authors are grateful to Rony Keppens for his help on the numerical aspects. E.R.P. is grateful to the UK Particle Physics and Astronomy Research Council and to the EU Solaire network for financial support. The contribution of T.G.F was supported by NSF Grant Nos. ATM-0518218 and ATM-0752257, and NASA Grant Nos. NNX08AG44G and NNX-06AC19G.

¹E. R. Priest and T. G. Forbes, *Magnetic Reconnection* (Cambridge University Press, Cambridge, 2000).

²H. E. Petschek, *AAS-NANA Symposium on the Physics of Solar Flares* (NASA, Washington, DC, 1964), NASA Spec. Publ. SP-50, p. 425.

³R. M. Kulsrud, *Earth, Planets Space* **53**, 417 (2001).

⁴D. Biskamp, *Nonlinear Magnetohydrodynamics* (Cambridge University Press, Cambridge, 1993).

⁵H. Baty, E. R. Priest, and T. G. Forbes, *Phys. Plasmas* **13**, 022312 (2006).

⁶P. A. Sweet, *Electromagnetic Phenomena in Cosmic Physics*, edited by B. Lenhart (Cambridge University Press, Cambridge, 1958), p. 135.

⁷E. N. Parker, *Phys. Rev.* **107**, 830 (1957).

⁸T. G. Forbes, *Earth, Planets Space* **53**, 423 (2001).

⁹G. Tóth, *Astrophys. Lett. Commun.* **34**, 245 (1996).

¹⁰P. Collela and P. R. Woodward, *J. Comput. Phys.* **54**, 174 (1984).

¹¹A. Harten, *J. Comput. Phys.* **49**, 357 (1983).

¹²R. B. Brackbill and D. C. Barnes, *J. Comput. Phys.* **35**, 426 (1980).

¹³M. Yan, L. C. Lee, and E. R. Priest, *J. Geophys. Res.* **97**, 8277, DOI 10.1029/92JA00170 (1992).

¹⁴M. Scholer, *J. Geophys. Res.* **94**, 8805, DOI: 10.1029/JA094iA07p08805 (1989).